Quantum compiling with a variational instruction set for accurate and fast quantum computing

Ying Lu,[1] Peng-Fei Zhou [⊕],[1] Shao-Ming Fei,[2,3,*] and Shi-Ju Ran [⊕][1,†]

[1]*Department of Physics, Capital Normal University, Beijing 100048, China*
[2]*School of Mathematical Sciences, Capital Normal University, Beijing 100048, China*
[3]*Max-Planck-Institute for Mathematics in the Sciences, 04103 Leipzig, Germany*

The quantum instruction set (QIS) is defined as the quantum gates that are physically realizable by controlling the qubits in quantum hardware. Compiling quantum circuits into the product of the gates in a properly defined QIS is a fundamental step in quantum computing. We here propose the quantum variational instruction set (QuVIS) formed by flexibly designed multiqubit gates for higher speed and accuracy of quantum computing. The controlling of qubits for realizing the gates in a QuVIS is variationally achieved using the fine-grained time optimization algorithm. Significant reductions in both the error accumulation and time cost are demonstrated in realizing the swaps of multiple qubits and quantum Fourier transformations, compared with the compiling by a standard QIS such as the quantum microinstruction set (QuMIS, formed by several one- and two-qubit gates including one-qubit rotations and controlled-NOT gates). With the same requirement on quantum hardware, the time cost for QuVIS is reduced to less than one-half of that for QuMIS. Simultaneously, the error is suppressed algebraically as the depth of the compiled circuit is reduced. As a general compiling approach with high flexibility and efficiency, QuVIS can be defined for different quantum circuits and be adapted to the quantum hardware with different interactions.

I. INTRODUCTION

Efficient compiling of quantum algorithms to physically executable forms belongs among the fundamental issues of quantum computing. A widely recognized compiling method is to transform the circuit into the product of executable elementary gates, which are named the quantum instruction set (QIS) [1–5]. A QIS should be constructed according to the fundamental physical mechanism of the quantum hardware. For instance, a superconducting quantum computer can adopt the quantum microinstruction set (QuMIS) [6] as the instructive set; it is formed by several one- and two-qubit gates including one-qubit rotations and controlled-NOT (CNOT) gates. For quantum photonic circuits, the elementary gates represent certain basic operations on single photons [7,8]. The efficiency of compiling a given quantum algorithm with a chosen QIS can be characterized by the complexity (e.g., depth) of the compiled circuit.

A typical way to realize the elementary gates in a QIS is by controlling the dynamics of the quantum hardware. Different quantum platforms are usually described by different controlling process. For instance, superconducting circuits

employ microwave-pulse techniques to manipulate the qubits [9,10] through, e.g., cross resonance [11], parametric modulation [12], etc. Another typical type of quantum hardware involves nuclear magnetic resonance (NMR) systems [13–21]. For such systems, a key issue in realizing quantum circuits or algorithms, such as Shor's factoring algorithm [22] and Harrow-Hassidim-Lloyd-related algorithms [23], is to determine the tunable time-dependent pulses. The efficiency can be characterized by the time cost of the controlling process.

For two-qubit gates, such as CNOT and SWAP gates, the optimal time cost has theoretically given bounds [24–26]. For N-qubit gates with $N > 2$, such bounds are not rigorously given in most cases, and variational methods including machine learning (ML) techniques have recently been adopted in such optimal-control problems [27–37]. Besides, quantum many-body systems have also been used to implement measurement-based quantum computation [38–44]. However, most conventional methods concern the controlling of a few qubits. The utilizations of the many-body dynamics for quantum computing [29,32,33,36,45–47] are much less explored due to the exponentially high complexity.

For all known quantum computing platforms, noise is inevitable and will induce computational errors that make the results unstable or unreliable. One way to fight against errors is to use error correction codes [48], such as Calderbank-Shor-Steane codes [49], Reed-Muller quantum codes [50], and toric codes [51]. However, the implementation of quantum error correction codes will significantly increase not only the number of qubits but also the complexity of circuits. This issue is particularly important in the noisy intermediate-scale quantum (NISQ) era, where the number of available qubits

---

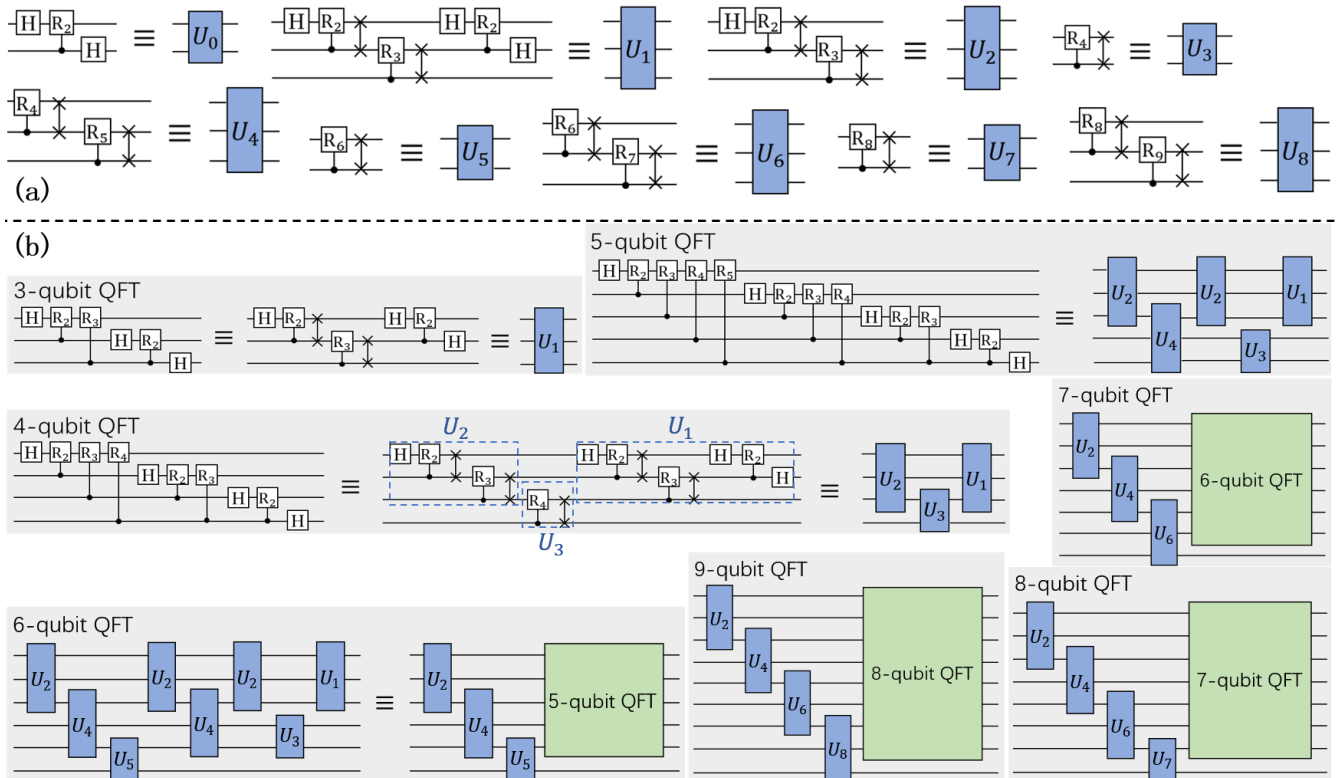*Corresponding author: feishm@cnu.edu.cn
†Corresponding author: sjran@cnu.edu.cn

FIG. 1. (a) The nine elementary gates $\{U_m\}$ ($m = 0, \ldots, 8$) in the three-qubit QuVIS for compiling the N-qubit QFT circuits for $N \leqslant 9$. We use "H" to denote a Hadamard gate, two crosses connected by a vertical line to denote a SWAP gate, and "R_p" connected to a dot to denote a controlled-phase-shift gate with the phase $\theta = \pi/2^p$. The error and the time used to implement each elementary gate are shown in Table I. By adding necessary SWAP gates, the N-qubit QFT circuits compiled by the three-qubit QuVIS are shown in (b).

and the connectivity between them are limited. Besides, noise will also lead to decoherence, meaning that the qubits will gradually become less entangled, losing the supremacy over classical computing. Prolonging the coherence time and reducing the time cost so that the quantum computing tasks are executed within the coherence duration belong to the significant and challenging issues for quantum computing in the NISQ era (see, e.g., Refs. [52–56]).

Aiming at higher efficiency and accuracy, we here propose the quantum variational instruction set (QuVIS) for compiling the quantum circuits. A QuVIS is defined as the flexibly designed multiqubit quantum gates that can be realized by controlling the magnetic pulses imposed on the interacting spins in quantum hardware. The pulse sequences are variationally determined using the fine-grained time optimization (FGTO) algorithm [36], which manages to efficiently realize the given multiqubit unitary transformations. We take QuMIS [6] as an example to compare the performances (error and time cost). Our results show that QuVIS significantly reduces the number of elementary gates in the compiled circuit, thus suppressing the accumulation of errors and the time cost. These advantages of QuVIS are demonstrated by compiling the circuits of N-qubit quantum Fourier transformation (QFT) [57–59] and multiqubit SWAP circuits. We show the elementary gates of the QuVIS designed for the N-qubit QFT in Fig. 1(a) and the compiled circuits for $N = 3, \ldots, 9$ in Fig. 1(b). Thanks to the generality and stability of FGTO in realizing unitary transformations, QuVIS can be adaptively

defined for different types of quantum hardware with various interaction types (e.g., Ising or Heisenberg interactions), connectivities, and strengths among the qubits, according to the quantum hardware considered.

II. VARIATIONAL INSTRUCTION SET

To realize a target unitary transformation $\hat{U}$, we optimize the adjustable parameters in the time-dependent Hamiltonian $\hat{H}(t)$ so that the time-evolution operator in the duration T optimally gives $\hat{U}$, i.e., $\hat{U} \simeq e^{-i\int_0^T \hat{H}(t)dt}$. We take the Planck constant $\hbar = 1$ for simplicity. In many of the existing types of quantum hardware, the adjustable parameters of the Hamiltonian concern the one-body terms, i.e., the magnetic pulses [16,17,60,61]. We here take the Ising model with time-dependent transverse fields for demonstration. The Ising Hamiltonian can be written as

$$\hat{H}(t) = \sum_{nn'} J_{nn'} \hat{S}_n^z \hat{S}_{n'}^z - 2\pi \sum_n \left[h_n^x(t)\hat{S}_n^x + h_n^y(t)\hat{S}_n^y \right], \quad (1)$$

with $\hat{S}_n^\alpha$ being the spin operator in the α direction ($\alpha = x, y, z$), $J_{nn'}$ being the coupling constants between the nth and n'th spins, and $h_n^\alpha(t)$ being the adjustable magnetic pulses along the spin-α direction on the nth spin at the time t. The goal becomes optimizing $h_n^\alpha(t)$ to minimize the difference

$$\varepsilon = |\hat{U} - e^{-i\int_0^T \hat{H}(t)dt}|, \quad (2)$$

where $|*|$ is the Frobenius norm. Such optimizations can be efficiently implemented by the gradient-descent methods even when $\hat{U}$ concerns multiple qubits.

Due to the generality of the optimization scheme, we are able to consider additional restrictions in the optimization process. For instance, we may introduce the restriction that only the magnetic field in either the x or y direction can be imposed at each time, or that the strength of magnetic fields should be limited to a certain range. Such restrictions (and many restrictions in realistic hardware) will not break the "automagical" differentiation chain and thus can be readily considered in the optimization.

We utilize the fine-grained time optimization (FGTO) [36] to optimize the pulse sequences for the target gates. The idea is to avoid being trapped in local minima by gradually fine-graining the time discretization. The validity of this strategy has been demonstrated on the state-preparation tasks. We take the Trotter-Suzuki form [62,63] and discretize the total time T to $\tilde{K}$ identical slices. The evolution operator can be approximated as

$$\hat{U}(T) = e^{-i\tilde{\tau}\hat{H}(\tilde{K}\tilde{\tau})} \cdots e^{-i\tilde{\tau}\hat{H}(2\tilde{\tau})} e^{-i\tilde{\tau}\hat{H}(\tilde{\tau})}, \qquad (3)$$

with $\tilde{\tau} = \frac{T}{\tilde{K}}$ controlling the Trotter-Suzuki error. To vary the magnetic fields, we introduce $\tau = \kappa\tilde{\tau}$, with κ being a positive integer, and assume $h_n^\alpha(t)$ to take the constant value $h_n^\alpha(t) = h_{n,k}^\alpha$ during the time $(k-1)\tau \leqslant t < k\tau$ (with $k = 1, \ldots, K$ and $K = \frac{T}{\tau}$). In other words, τ controls the maximal frequency of the magnetic pulses, and the magnetic fields are allowed to change K times in the controlling duration. During the optimization, τ is reduced gradually to increase the fineness of time discretization. We start from a relatively large τ and reduce it to $\tau/2$ when $\{h_{n,k}^\alpha\}$ converge. The length (i.e., the dimension of the index k) of the pulse sequences will be doubled. At the beginning of the optimization with a new (smaller) τ, the pulse sequences are initialized as $h_{n,2k'-1}^\alpha = h_{n,2k'}^\alpha \leftarrow h_{n,k'}^\alpha$.

The magnetic fields are updated as

$$h_{n,k}^\alpha \leftarrow h_{n,k}^\alpha - \eta \frac{\partial \varepsilon}{\partial h_{n,k}^\alpha}, \qquad (4)$$

where the gradients $\frac{\partial \varepsilon}{\partial h_{n,k}^\alpha}$ can be obtained by, e.g., the automatic differentiation technique in PYTORCH [64]. We use the optimizer ADAM [65] to dynamically control the learning rate η.

The QuVIS for different quantum circuits can be defined flexibly. Specifically, we call a QuVIS an $\tilde{N}$-qubit QuVIS when the elementary gates within it are at most $\tilde{N}$-qubit gates. Let us take the QFT as an example, which is one of the most frequently used circuits in implementing quantum algorithms including the Shor [66] and Grover algorithms [67]. Figure 1(a) gives the three-qubit QuVIS for the N-qubit QFT with $N \leqslant 9$, and Fig. 1(b) shows the circuits after compiling. The magnetic fields to realize each elementary gate are obtained by the algorithm explained above.

The complexity of obtaining the magnetic fields on a classical computer (i.e., optimization complexity) increases exponentially with $\tilde{N}$ (the maximal number of qubits in the elementary gates of QuVIS). This optimization complexity is independent of the number of qubits N in the circuit that is to

be compiled. In comparison, we may consider the whole quantum circuit as a large unitary transformation and use FGTO to minimize the distance between this unitary transformation and the time-evolution operator. We dub such a simple and brute-force scheme "direct control," which will be used later as a baseline. In this case, we need to simulate the time evolution of an N-qubit system; thus the optimization complexity of the direct control scheme increases exponentially with N.

Here, we focus on the QuVIS with $\tilde{N} = 2$ and 3, which already exhibits significant advantages in terms of efficiency and accuracy (see the benchmark results). Be aware that one can use a desktop computer to access the QuVISs for $\tilde{N} \leqslant 6$ without any problems. QuVIS can also be designed flexibly for different quantum circuits or algorithms other than QFT. More details on the optimization and the controlling sequences for realizing the elementary gates of QuVIS can be found in the Supplemental Material [68].

The elementary gates (or most of them) in a QuVIS can be derived recursively. Taking the QuVIS for QFT as an example, the elementary gates from U_0 to U_2 are designed manually. Clear regularity appears to derive the rest of gates recursively. For the definitions of the elementary gates in QuVIS, the mth gate U_m is composed of the rotational gate R_{m+1} and a SWAP gate when m is odd. For an even m, U_m is composed of two rotational gates (R_{m+1} and R_m) and two SWAP gates; see Figs. 2(a) and 2(b). When compiling the N-qubit QFT by QuVIS, the circuit consists of $U_2, U_4, U_6, \ldots, U_{N-5}, U_{N-3}, U_{N-1}$ and the $(N-1)$-qubit QFT circuit, when N is odd [Fig. 2(c)]. When N is even, the N-qubit QFT circuit consists of $U_2, U_4, U_6, \ldots, U_{N-4}, U_{N-2}, U_{N-1}$ and the $(N-1)$-qubit QFT circuit [Fig. 2(d)].

III. BENCHMARK RESULTS

Below, we take the Hamiltonian for time evolution to be the nearest-neighbor Ising chain, where the coupling constants satisfy

$$J_{nn'} = \begin{cases} 2\pi & \text{for } n' = n+1 \\ 0 & \text{otherwise.} \end{cases} \qquad (5)$$

In our demonstration, we fix the magnetic fields along the spin-z direction as zero and allow the fields to be independently adjusted along the spin-x and spin-y directions. Such a case often appears in situations involving control using radio-frequency pulses [17,69].

Table I shows the time cost T for realizing the elementary gates $\{\hat{U}_m\}$ ($m = 0, \ldots, 8$) by FGTO (first row of data). For comparison, we also estimate the time cost by compiling each gate into the product of the elementary gates in QuMIS (second row of data). To conveniently and fairly compare the time cost, we take the T when the error [Eq. (2)] decreases to about $O(10^{-2})$. The time cost of implementing the elementary gate in the QuVIS using FGTO is significantly lower than that when compiling them into the product of the elementary gates in QuMIS. Note that in general the loss function will decrease as the total time duration T increases, until the limit of the optimization scheme is reached. Such a limit is determined by many factors including the gradient step (learning rate) and other optimization tricks (such as the optimizer, for which we
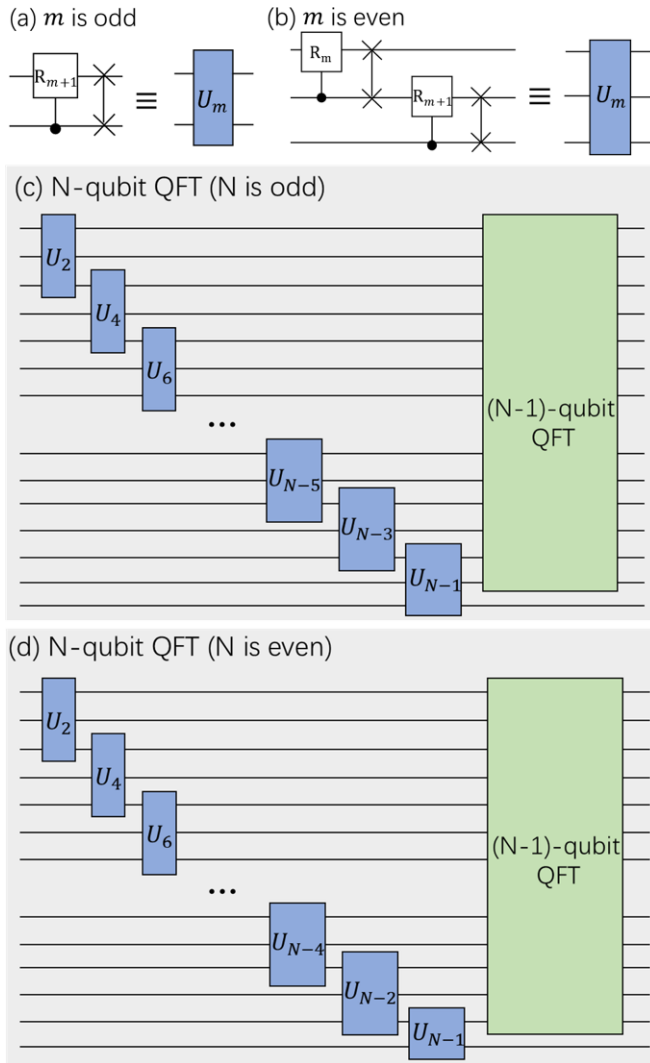
FIG. 2. The elementary gates for compiling the QFT circuits with three-qubit QuVIS can be recursively derived. (a) and (b) show the definitions of the mth elementary gate U_m for $m \geqslant 3$ with odd and even m, respectively. The circuit after compiling the N-qubit QFT circuit can also be derived as illustrated in (c) for odd N and (d) for even N.

choose adaptive moment estimation [70]). In our simulations, the loss function eventually converges to about $O(10^{-6})$ (see Fig. S2 in the Supplemental Material).

In Fig. 3, we demonstrate the time costs T and the error ε in realizing the circuits for N-qubit QFT. The direct control

TABLE I. The time cost T to implement the elementary gates $\{\hat{U}_m\}$ ($m = 0, \ldots, 8$) of the three-qubit QuVIS [Fig. 1(a)] for QFT. The first row of data shows the results obtained by directly taking $\{\hat{U}_m\}$ as the target gates in Eq. (2), and the second row of data shows those obtained by compiling $\{\hat{U}_m\}$ into the product of the elementary gates in QuMIS.

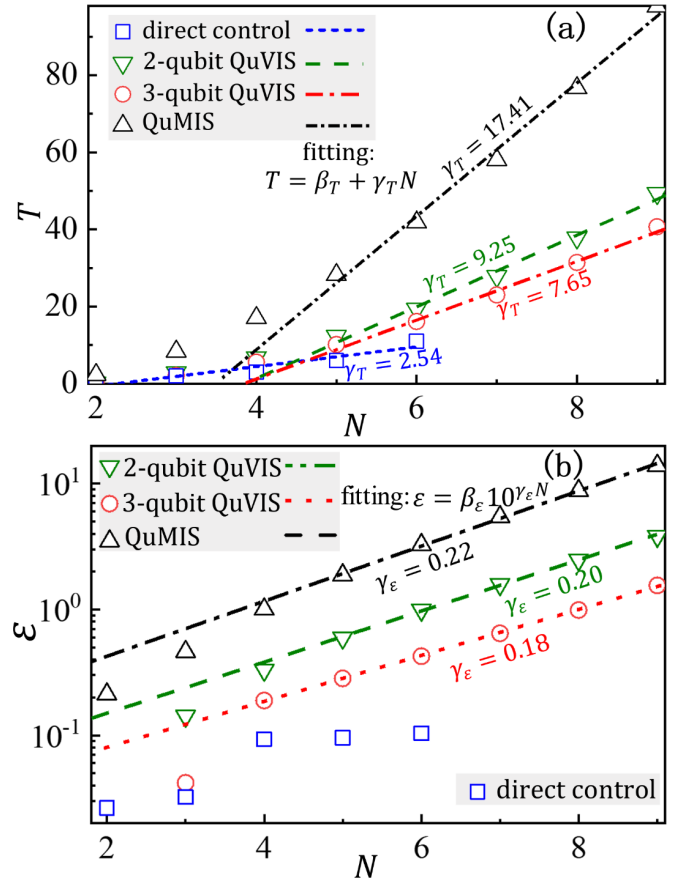| T	$\hat{U}_0$	$\hat{U}_1$	$\hat{U}_2$	$\hat{U}_3$	$\hat{U}_4$	$\hat{U}_5$	$\hat{U}_6$	$\hat{U}_7$	$\hat{U}_8$
QuVIS	0.3	2.1	2.1	1.4	2.4	1.5	2.4	1.5	2.4
QuMIS	2.3	8.4	6.0	2.6	5.1	2.5	5.0	2.5	5.0

FIG. 3. (a) The time cost T and (b) the error ε in realizing the N-qubit QFT using direct control, two-qubit QuVIS, three-qubit QuVIS, and QuMIS. The various dashed lines give the linear fitting of the time cost T vs N [Eq. (6)]. In the optimization for direct control, the time cost is estimated under the condition that ε is no more than 10^{-1}. For the two-qubit QuVIS, three-qubit QuVIS, and QuMIS, ε changes exponentially with N [Eq. (7)]. Note that the fittings are performed using the data for $N \geqslant 5$.

scheme is used as a baseline method to compare with QuVIS and QuMIS. Though it exhibits the lowest error, its disadvantage is that the computational cost increases exponentially with the number of qubits N in the quantum circuit to be compiled. Thus it is not feasible to apply it to circuits of large size.

Compared with QuMIS, significant reductions in both the time cost T and the error ε are demonstrated when using the two- and three-qubit QuVISs for compiling. Since T is determined by the number of elementary gates and the time to realize each of them, it is approximately linear with the number of qubits N. We have

$$T = \gamma_T N + \beta_T, \qquad (6)$$

with the slopes $\gamma_T \simeq 17.41$, 9.25, and 7.65 for QuMIS, $\tilde{N}$-qubit QuVIS with $\tilde{N} = 2$, and $\tilde{N}$-qubit QuVIS with $\tilde{N} = 3$, respectively.

Since each elementary gate inevitably introduces certain error [fixed to be $O(10^{-2})$ in our simulations], the error ε for the whole circuit generally accumulates exponentially as N
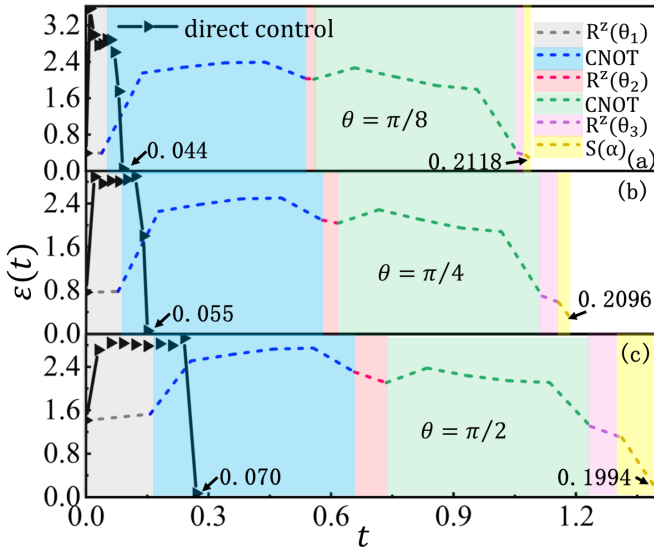
FIG. 4. The error $\varepsilon(t)$ [Eq. (8)] vs the evolution time t to realize the controlled-phase-shift gate [Eq. (9)]. The dashed lines and the solid lines with triangles show the $\varepsilon(t)$ obtained using QuMIS and direct control, respectively. The colored shading indicates the time cost for realizing the gates on the right-hand side of Eq. (10).

increases. We have

$$\varepsilon = \beta_\varepsilon e^{\gamma_\varepsilon N}, \qquad (7)$$

with the exponent coefficients $\gamma_\varepsilon = 0.22$, 0.2, and 0.18 for QuMIS, $\tilde{N}$-qubit QuVIS with $\tilde{N} = 2$, and $\tilde{N}$-qubit QuVIS with $\tilde{N} = 3$. A reduction in γ_ε indicates an algebraic improvement, essentially because the number of elementary gates (i.e., the depth) of the compiled circuit is reduced by increasing $\tilde{N}$.

The key advantage of QuVIS is the "end-to-end" optimization strategy for the magnetic pulses. When a unitary transformation is compiled into the product of several gates, the conventional schemes require accurate implementations of all gates. However, we actually care about the unitary transformation itself, not any intermediate results within the compiled circuit.

An $\tilde{N}$-qubit QuVIS is designed by dividing the target circuit into many subcircuits [Fig. 1(b)], where each subcircuit has at most $\tilde{N}$ qubits and the total number of subcircuits should be as small as possible. These subcircuits define the elementary gates in the QuVIS [Fig. 1(a)]. The magnetic pulses are optimized by directly finding the optimal path to each elementary gate, without considering the intermediate results within the corresponding subcircuit. Meanwhile, a properly designed QuVIS will significantly reduce the number of elementary gates in a compiled circuit. For these reasons, a circuit compiled by a QuVIS exhibits much less error and lower time cost compared with one compiled by a standard QIS.

To provide an explicit demonstration, we show in Fig. 4 the error $\varepsilon(t)$ in the controlling duration

$$\varepsilon(t) = |\hat{U}(\theta) - e^{-i \int_0^t \hat{H}(t')dt'}|. \qquad (8)$$

This quantity gives the distance at a certain time point t with $0 \leqslant t \leqslant T$, where the magnetic fields are still optimized by

minimizing $\varepsilon(T)$ [Eq. (2)]. As an example, we take $\hat{U}(\theta)$ to be the controlled-phase-shift gate

$$\hat{U}(\theta) = \begin{bmatrix} 1 & 0 & 0 & 0 \\ 0 & 1 & 0 & 0 \\ 0 & 0 & 1 & 0 \\ 0 & 0 & 0 & e^{i\theta} \end{bmatrix}. \qquad (9)$$

For the phase shifts $\theta = \frac{\pi}{8}$, $\frac{\pi}{4}$, and $\frac{\pi}{2}$, Fig. 4 compares the error $\varepsilon(t)$ [Eq. (8)] obtained when directly minimizing the distance to the target gate (direct control) and when using the standard compiling. Using QuMIS, $\hat{U}(\theta)$ is decomposed into the product of the single-qubit rotation gates $\hat{R}^z$ and CNOT gates $\hat{C}$, which can be formally written as

$$\hat{U}(\theta) = \hat{S}(\alpha)\hat{R}^z(\theta_1)\hat{C}\hat{R}^z(\theta_2)\hat{C}\hat{R}^z(\theta_3), \qquad (10)$$

where $\hat{R}^z(\theta_1)$, $\hat{R}^z(\theta_2)$, and $\hat{R}^z(\theta_3)$ are single-qubit rotations along the spin-z direction satisfying $\hat{R}^z(\theta_1)\hat{R}^z(\theta_2)\hat{R}^z(\theta_3) = I$ and $\hat{S}(\alpha) = e^{i\alpha}$ a phase factor [71]. Note that all single-qubit gates in Eq. (10) act on the second qubit. In other words, when the control qubit (the first one here) is in the state $|1\rangle$, the target qubit (the second one) will be acted
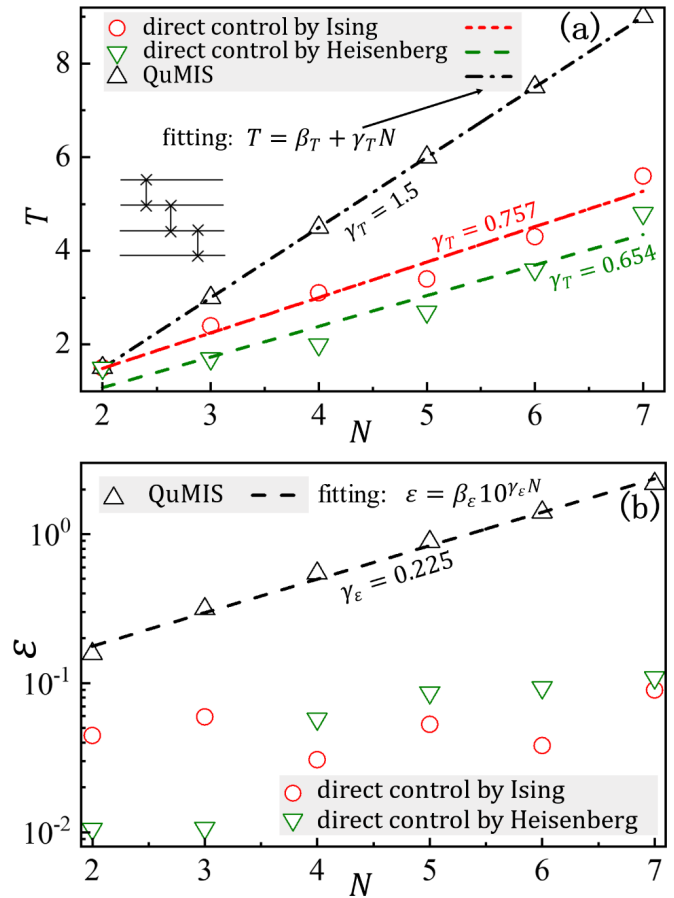

FIG. 5. (a) The time cost T and (b) the corresponding error ε for the N-qubit SWAP circuit using direct control with Ising and Heisenberg interactions. The inset in (a) illustrates the circuit for a four-qubit swap. The data for QuMIS with Ising interactions are also given for comparison. The fitting functions of T and ε are given in Eqs. (6) and (7), respectively.

on by $\hat{S}(\alpha)\hat{R}^z(\theta_1)\hat{X}\hat{R}^z(\theta_2)\hat{X}\hat{R}^z(\theta_3)$, with $\hat{X}$ being the Pauli-X operator.

The time costs of realizing the elementary gates in QuMIS are illustrated by the colored shading in Fig. 4. The time cost of direct control is indicated by the x coordinate of the last triangle, which is about five times shorter than QuMIS. Note that for a single-qubit rotation $\hat{R}^\alpha(\theta)$, it can be written as the one-body evolution operator with the magnetic field along the corresponding direction, i.e., $\hat{R}^\alpha(\theta) = e^{-i\theta\hat{S}^\alpha} \Leftrightarrow \hat{U}(h^\alpha, T) = e^{-iTh^\alpha\hat{S}^\alpha}$. Therefore the time cost of $\hat{R}^\alpha(\theta)$ is estimated as $T = \frac{\theta}{h^\alpha}$. Without losing generality, we here take $h^\alpha = 10$ to estimate the time costs of single-qubit rotations.

An important observation is that even the time cost of a single CNOT gate ($T = 0.5$ theoretically given in Refs. [25,26]) is larger than that of $\hat{U}(\theta)$ obtained using direct control. Meanwhile, direct control also exhibits much lower errors with $\varepsilon \sim O(10^{-2})$. For QuMIS, the error accumulates and finally reaches $O(10^{-1})$, which is about ten times larger than that obtained using direct control. Therefore, from the perspective of QuVIS, it becomes less efficient and accurate when decomposing the $\hat{U}(\theta)$ into the product of CNOT gates and the single-qubit rotations.

The pulse sequences can be optimized for the quantum platforms with different interactions. Figure 5 shows the time cost T and the corresponding error ε for the N-qubit SWAP circuit using direct control with Ising and Heisenberg interactions. The circuit swaps the first qubit with the last [see the inset of Fig. 5(a)]. The time T is estimated by keeping the error of each elementary gate to $O(10^{-1})$ or less. Linear scaling of T given by Eq. (6) is observed for both kinds of interactions. Thanks to the flexibility of the optimization algorithm, pulse sequences can be obtained for any type or strength of the interactions, and the error of realizing the elementary gates can be readily estimated.

IV. SUMMARY

We here propose the quantum variational instruction set (QuVIS) for efficient quantum computing based on the dynamics of the interacting spin systems controlled by pulse sequences of magnetic fields. The key idea of QuVIS is to flexibly define the multiqubit elementary gates, where we ignore the intermediate processes but optimize the magnetic fields to directly realize the target unitary transformations. By taking the N-qubit quantum Fourier transformation as an example, significant reductions in the time cost and error accumulation are demonstrated compared with the standard quantum instruction set. QuVIS provides a flexible quantum compiling scheme generally for quantum platforms with known interactions. For cases where the interactions are unknown, one can combine QuVIS with methods that estimate the interactions using, e.g., machine learning of the local observables and reduced density matrices [72–74].

[1] A. S. Green, P. L. Lumsdaine, N. J. Ross, P. Selinger, and B. Valiron, Quipper: A scalable quantum programming language, in *Proceedings of the 34th ACM SIGPLAN Conference on Programming Language Design and Implementation* (ACM Press, New York, 2013), pp. 333–342.

[2] D. Wecker and K. M. Svore, LIQUi|>: A software design architecture and domain-specific language for quantum computing, arXiv:1402.4467.

[3] A. JavadiAbhari, S. Patil, D. Kudrow, J. Heckey, A. Lvov, F. T. Chong, and M. Martonosi, ScaffCC: Scalable compilation and analysis of quantum programs, Parallel Comput. **45**, 2 (2015).

[4] F. T. Chong, D. Franklin, and M. Martonosi, Programming languages and compiler design for realistic quantum hardware, Nature (London) **549**, 180 (2017).

[5] T. Häner, D. S. Steiger, K. Svore, and M. Troyer, A software methodology for compiling quantum programs, Quantum Sci. Technol. **3**, 020501 (2018).

[6] X. Fu, M. A. Rol, C. C. Bultink, J. Van Someren, N. Khammassi, I. Ashraf, R. Vermeulen, J. De Sterke, W. Vlothuizen, R. Schouten, C. G. Almudever, L. DiCarlo, and K. Bertels, An experimental microarchitecture for a superconducting quantum processor, in *Proceedings of the 50th Annual IEEE/ACM International Symposium on Microarchitecture* (ACM Press, New York, 2017), pp. 813–825.

[7] J. L. O'Brien, A. Furusawa, and J. Vučković, Photonic quantum technologies, Nat. Photon. **3**, 687 (2009).

[8] A. Aspuru-Guzik and P. Walther, Photonic quantum simulators, Nat. Phys. **8**, 285 (2012).

[9] P. Krantz, M. Kjaergaard, F. Yan, T. P. Orlando, S. Gustavsson, and W. D. Oliver, A quantum engineer's guide to superconducting qubits, Appl. Phys. Rev. **6**, 021318 (2019).

[10] D. C. McKay, S. Filipp, A. Mezzacapo, E. Magesan, J. M. Chow, and J. M. Gambetta, Universal Gate for Fixed-Frequency Qubits via a Tunable Bus, Phys. Rev. Appl. **6**, 064007 (2016).

[11] J. M. Chow, A. D. Córcoles, J. M. Gambetta, C. Rigetti, B. R. Johnson, J. A. Smolin, J. R. Rozen, G. A. Keefe, M. B. Rothwell, M. B. Ketchen, and M. Steffen, Simple All-Microwave Entangling Gate for Fixed-Frequency Superconducting Qubits, Phys. Rev. Lett. **107**, 080502 (2011).

[12] M. Reagor, C. B. Osborn, N. Tezak, A. Staley, G. Prawiroatmodjo, M. Scheer, N. Alidoust, E. A. Sete, N. Didier, M. P. da Silva, E. Acala, J. Angeles, A. Bestwick, M. Block, B. Bloom, A. Bradley, C. Bui, S. Caldwell, L. Capelluto, R. Chilcott *et al.*, Demonstration of universal parametric

entangling gates on a multi-qubit lattice, Sci. Adv. **4**, eaao3603 (2018).

[13] D. G. Cory, M. D. Price, and T. F. Havel, Nuclear magnetic resonance spectroscopy: An experimentally accessible paradigm for quantum computing, Phys. D (Amsterdam) **120**, 82 (1998).

[14] J. A. Jones, R. Hansen, and M. Mosca, Quantum logic gates and nuclear magnetic resonance pulse sequences, J. Magn. Reson. **135**, 353 (1998).

[15] J. A. Jones and M. Mosca, Implementation of a quantum algorithm on a nuclear magnetic resonance quantum computer, J. Chem. Phys. **109**, 1648 (1998).

[16] L. M. Vandersypen, M. Steffen, G. Breyta, C. S. Yannoni, M. H. Sherwood, and I. L. Chuang, Experimental realization of Shor's quantum factoring algorithm using nuclear magnetic resonance, Nature (London) **414**, 883 (2001).

[17] L. M. K. Vandersypen and I. L. Chuang, NMR techniques for quantum control and computation, Rev. Mod. Phys. **76**, 1037 (2005).

[18] J. Bian, M. Jiang, J. Cui, X. Liu, B. Chen, Y. Ji, B. Zhang, J. Blanchard, X. Peng, and J. Du, Universal quantum control in zero-field nuclear magnetic resonance, Phys. Rev. A **95**, 052342 (2017).

[19] I. L. Chuang, N. Gershenfeld, and M. Kubinec, Experimental Implementation of Fast Quantum Searching, Phys. Rev. Lett. **80**, 3408 (1998).

[20] J. A. Jones, Fast searches with nuclear magnetic resonance computers, Science **280**, 229 (1998).

[21] J. Zhang, Z. Lu, L. Shan, and Z. Deng, Realization of generalized quantum searching using nuclear magnetic resonance, Phys. Rev. A **65**, 034301 (2002).

[22] P. W. Shor, Polynomial-time algorithms for prime factorization and discrete logarithms on a quantum computer, SIAM Rev. **41**, 303 (1999).

[23] A. W. Harrow, A. Hassidim, and S. Lloyd, Quantum Algorithm for Linear Systems of Equations, Phys. Rev. Lett. **103**, 150502 (2009).

[24] N. Khaneja, R. Brockett, and S. J. Glaser, Time optimal control in spin systems, Phys. Rev. A **63**, 032308 (2001).

[25] B. Li, Z. Yu, S. Fei, and X. Li-Jost, Time optimal quantum control of two-qubit systems, Sci. China: Phys. Mech. Astron. **56**, 2116 (2013).

[26] B.-Z. Sun, S.-M. Fei, N. Jing, and X. Li-Jost, Time optimal control based on classification of quantum gates, Quantum Inf. Process. **19**, 103 (2020).

[27] K. G. Kim and M. D. Girardeau, Optimal control of strongly driven quantum systems: Fully variational formulation and nonlinear eigenfields, Phys. Rev. A **52**, R891 (1995).

[28] N. Leung, M. Abdelhafez, J. Koch, and D. Schuster, Speedup for quantum optimal control from automatic differentiation based on graphics processing units, Phys. Rev. A **95**, 042318 (2017).

[29] Z.-C. Yang, A. Rahmani, A. Shabani, H. Neven, and C. Chamon, Optimizing Variational Quantum Algorithms Using Pontryagin's Minimum Principle, Phys. Rev. X **7**, 021027 (2017).

[30] V. Cavina, A. Mari, A. Carlini, and V. Giovannetti, Variational approach to the optimal control of coherently driven, open quantum system dynamics, Phys. Rev. A **98**, 052125 (2018).

[31] R.-B. Wu, X. Cao, P. Xie, and Y.-X. Liu, End-To-End Quantum Machine Learning Implemented with Controlled Quantum Dynamics, Phys. Rev. Appl. **14**, 064020 (2020).

[32] A. Choquette, A. Di Paolo, P. K. Barkoutsos, D. Sénéchal, I. Tavernelli, and A. Blais, Quantum-optimal-control-inspired ansatz for variational quantum algorithms, Phys. Rev. Res. **3**, 023092 (2021).

[33] A. B. Magann, C. Arenz, M. D. Grace, T.-S. Ho, R. L. Kosut, J. R. McClean, H. A. Rabitz, and M. Sarovar, From pulses to circuits and back again: A quantum optimal control perspective on variational quantum algorithms, PRX Quantum **2**, 010101 (2021).

[34] D. Castaldo, M. Rosa, and S. Corni, Quantum optimal control with quantum computers: A hybrid algorithm featuring machine learning optimization, Phys. Rev. A **103**, 022613 (2021).

[35] Z. An, H.-J. Song, Q.-K. He, and D. L. Zhou, Quantum optimal control of multilevel dissipative quantum systems with reinforcement learning, Phys. Rev. A **103**, 012404 (2021).

[36] Y. Lu, Y.-M. Li, P.-F. Zhou, and S.-J. Ran, Preparation of many-body ground states by time evolution with variational microscopic magnetic fields and incomplete interactions, Phys. Rev. A **104**, 052413 (2021).

[37] I. Khait, J. Carrasquilla, and D. Segal, Optimal control of quantum thermal machines using machine learning, Phys. Rev. Res. **4**, L012029 (2022).

[38] G. K. Brennen and A. Miyake, Measurement-Based Quantum Computer in the Gapped Ground State of a Two-Body Hamiltonian, Phys. Rev. Lett. **101**, 010502 (2008).

[39] S. Benjamin, B. Lovett, and J. Smith, Prospects for measurement-based quantum computing with solid state spins, Laser Photon. Rev. **3**, 556 (2009).

[40] D. V. Else, I. Schwarz, S. D. Bartlett, and A. C. Doherty, Symmetry-Protected Phases for Measurement-Based Quantum Computation, Phys. Rev. Lett. **108**, 240505 (2012).

[41] K. Fujii and T. Morimae, Topologically protected measurement-based quantum computation on the thermal state of a nearest-neighbor two-body Hamiltonian with spin-3/2 particles, Phys. Rev. A **85**, 010304(R) (2012).

[42] A. S. Darmawan, G. K. Brennen, and S. D. Bartlett, Measurement-based quantum computation in a two-dimensional phase of matter, New J. Phys. **14**, 013023 (2012).

[43] T.-C. Wei and R. Raussendorf, Universal measurement-based quantum computation with spin-2 Affleck-Kennedy-Lieb-Tasaki states, Phys. Rev. A **92**, 012310 (2015).

[44] T.-C. Wei and C.-Y. Huang, Universal measurement-based quantum computation in two-dimensional symmetry-protected topological phases, Phys. Rev. A **96**, 032317 (2017).

[45] G. Passarelli, R. Fazio, and P. Lucignano, Optimal quantum annealing: A variational shortcut-to-adiabaticity approach, Phys. Rev. A **105**, 022618 (2022).

[46] J. Leng, Y. Peng, Y.-L. Qiao, M. Lin, and X. Wu, in *Differentiable analog Quantum Computing for Optimization and Control, in NeurIPS 2022*, Advances in Neural Information Processing Systems Vol. 35 (Curran Associates, Red Hook, NY, 2022), pp. 4707–4721.

[47] T. Huang, Y. Ding, L. Dupays, Y. Ban, M.-H. Yung, A. del Campo, and X. Chen, Time-optimal quantum driving by variational circuit learning, arXiv:2211.00405.

[48] D. A. Lidar and T. A. Brun, *Quantum Error Correction* (Cambridge University Press, New York, 2013).

[49] A. R. Calderbank and P. W. Shor, Good quantum error-correcting codes exist, Phys. Rev. A **54**, 1098 (1996).

[50] A. Steane, Quantum Reed-Muller codes, IEEE Trans. Inf. Theory **45**, 1701 (1999).

[51] A. Kitaev, Fault-tolerant quantum computation by anyons, Ann. Phys. (Amsterdam) **303**, 2 (2003).

[52] P. W. Shor, Scheme for reducing decoherence in quantum computer memory, Phys. Rev. A **52**, R2493 (1995).

[53] I. L. Chuang, R. Laflamme, P. W. Shor, and W. H. Zurek, Quantum computers, factoring, and decoherence, Science **270**, 1633 (1995).

[54] L.-M. Duan and G.-C. Guo, Reducing decoherence in quantum-computer memory with all quantum bits coupling to the same environment, Phys. Rev. A **57**, 737 (1998).

[55] A. Beige, D. Braun, B. Tregenna, and P. L. Knight, Quantum Computing Using Dissipation to Remain in a Decoherence-Free Subspace, Phys. Rev. Lett. **85**, 1762 (2000).

[56] J. Preskill, Quantum computing in the NISQ era and beyond, Quantum **2**, 79 (2018).

[57] A. Ekert and R. Jozsa, Quantum computation and Shor's factoring algorithm, Rev. Mod. Phys. **68**, 733 (1996).

[58] R. Jozsa, Quantum algorithms and the Fourier transform, Proc. R. Soc. London Ser. A **454**, 323 (1998).

[59] Y. S. Weinstein, M. A. Pravia, E. M. Fortunato, S. Lloyd, and D. G. Cory, Implementation of the Quantum Fourier Transform, Phys. Rev. Lett. **86**, 1889 (2001).

[60] M. Y. Niu, S. Boixo, V. N. Smelyanskiy, and H. Neven, Universal quantum control through deep reinforcement learning, npj Quantum Inf. **5**, 33 (2019).

[61] Y. Baum, M. Amico, S. Howell, M. Hush, M. Liuzzi, P. Mundada, T. Merkh, A. R. R. Carvalho, and M. J. Biercuk, Experimental deep reinforcement learning for error-robust gate-set design on a superconducting quantum computer, PRX Quantum **2**, 040324 (2021).

[62] H. F. Trotter, On the product of semi-groups of operators, Proc. Am. Math. Soc. **10**, 545 (1959).

[63] M. Suzuki, Generalized Trotter's formula and systematic approximants of exponential operators and inner derivations with applications to many-body problems, Commun. Math. Phys. **51**, 183 (1976).

[64] See the official website of PYTORCH at https://pytorch.org/.

[65] D. P. Kingma and J. Ba, Adam: A method for stochastic optimization, in *Proceedings of the 3rd International Conference on Learning Representations, ICLR 2015, San Diego, CA, USA, Conference Track*, edited by Y. Bengio and Y. LeCun (ICLR, Appleton, WI, 2015).

[66] P. Shor, Algorithms for quantum computation: discrete logarithms and factoring, in *Proceedings of the 35th Annual Symposium on Foundations of Computer Science* (IEEE Computer Society, Washington, DC, 1994), pp. 124–134.

[67] L. K. Grover, Quantum Mechanics Helps in Searching for a Needle in a Haystack, Phys. Rev. Lett. **79**, 325 (1997).

[68] See Supplemental Material at http://link.aps.org/supplemental/10.1103/PhysRevResearch.5.023096 for more details on realizing the QFT circuits using QuVIS and direct control.

[69] J. Li, R. Fan, H. Wang, B. Ye, B. Zeng, H. Zhai, X. Peng, and J. Du, Measuring Out-of-Time-Order Correlators on a Nuclear Magnetic Resonance Quantum Simulator, Phys. Rev. X **7**, 031011 (2017).

[70] D. P. Kingma and J. Ba, Adam: A method for stochastic optimization, arXiv:1412.6980.

[71] A. Barenco, C. H. Bennett, R. Cleve, D. P. DiVincenzo, N. Margolus, P. Shor, T. Sleator, J. A. Smolin, and H. Weinfurter, Elementary gates for quantum computation, Phys. Rev. A **52**, 3457 (1995).

[72] T. Xin, S. Lu, N. Cao, G. Anikeeva, D. Lu, J. Li, G. Long, and B. Zeng, Local-measurement-based quantum state tomography via neural networks, npj Quantum Inf. **5**, 109 (2019).

[73] X.-Y. Li, F. Lou, X.-G. Gong, and H. Xiang, Constructing realistic effective spin Hamiltonians with machine learning approaches, New J. Phys. **22**, 053036 (2020).

[74] X. Ma, Z. C. Tu, and S.-J. Ran, Deep learning quantum states for Hamiltonian estimation, Chin. Phys. Lett. **38**, 110301 (2021).